Hindawi
Geofluids
Volume 2022, Article ID 9385352, 9 pages
https://doi.org/10.1155/2022/9385352

Research Article

Recognition of Red-Bed Landslides over Eastern Sichuan through Remote Sensing and Field Investigations

Zhao Miao[1], **Panpan Tang**[2,3] **and Yong Zhang**[1]

[1]*Institute of Exploration Technology, Chinese Academy of Geological Sciences, Cheng Du, 611734 Sichuan, China*
[2]*Research Center of Big Data Technology, Nanhu Laboratory, Zhejiang 314002, China*
[3]*Advanced Institute of Big Data, Beijing 100093, China*

Correspondence should be addressed to Panpan Tang; tangpp@nanhulab.ac.cn

Received 24 January 2022; Revised 12 March 2022; Accepted 17 March 2022; Published 6 April 2022

Academic Editor: Wen-long Shen

Red-bed soft rock, characterized by the gentle slope, low intensity, and weak weathering resistance, is widely distributed over the Eastern Sichuan Province, China, threatening many lives of people, economy development, and urbanization progress. In this study, Multi-Temporal Synthetic Aperture Radar interferometry (MTInSAR) techniques and detailed field investigations were carried out to detect the potential red-bed landslides. The strategies of small baselines, phase optimization, and atmospheric delay removal were proved to be effective in improving the deformation results. Finally, dozens of slow-moving slopes were found and attributed to frequent human activities, and the applicability of various monitoring tools and the comparisons of their results were discussed. This research is aimed at proving the applicability of remote sensing measures in the monitoring of landslides, increasing the efficiency of this method, and helping the hazard prevention in Southwest China.

1. Introduction

Red beds refer to the continental sedimentary rocks composed of red mudstone, sandstone, siltstone, and shale, with the hard layer and soft layer alternately distributed in the vertical plane [1]. Most of them were formed in periods of the Jurassic, Cretaceous, or Tertiary and are usually in low intensity and vulnerable to the erosion of adverse weather. The red beds are widespread over the eastern Sichuan Basin of China, which is characterized by high mountains and abundant precipitation [2]. Although the red beds here are usually gentle with the dip angles smaller than 10° [3], they are still highly susceptible to landslides [4, 5]. This phenomenon is mainly attributed to the monsoon climate, weak geologic conditions, frequent engineering activities, and massive loose deposits (such as residual, alluvial, diluvial, and colluvial deposits) accumulated on the shallow layers [2, 6]. Various environmental factors can lead to displacement [7]. The most direct cause is the continual or heavy rainfall, which will increase the sliding stress and intenerate the clay mineral to decrease the effective stress and shear strength of the failure slope sharply [8].

According to statistics, the red-bed kind landslides account for approximately one quarter of all landslides in the Western China [9]. Especially in 1989, there were more than 10000 landslides triggered by an extensive rainfall exceeding 200 mm [10]. From 2008 to 2011, the frequency of geological disasters in this region was very high, and thousands of landslides occurred every year, including several huge ones. These landslides are usually clustered, concealed, sudden, and extremely destructive [9, 11], causing many casualties and destructions of houses and infrastructures. Moreover, a large number of residences and engineering projects under threat have to be entirely moved. As well as rainfall, soil property is an import factor affecting the distribution of landslides [12].

The early identification of landslides is helpful to the hazard prevention and management of the construction activities. A thorough field investigation, including traditional methods like leveling, GPS, and geophysical prospect-

ing, is difficult and time/money consuming because of the large scale of landslide distribution and complex topography. In contrast, remote sensing (synthetic aperture radar (SAR) and optical) is a more effective tool owning to its high resolution, broad coverage, and short revisiting period [13–15]. The satellite SAR images, available in all-weather and day-night, have played a key role in identifying the potential hazard due to its capability of high-precise deformation monitoring (cm to mm range). There are many methods based on the satellite SAR images, such as Permanent Scatterers (PSInSAR) [16], Small Baseline Subset (SBAS) [17], and SqueeSAR [18]. They have been successfully applied in many experiments [19–21], and these techniques are collectively referred to as Multi-Temporal differential SAR interferometry (MTInSAR). As a complement the optical image can be used in the understanding and interpretation of landslides at different stages, as its texture pattern and tone are almost identical to that observed by the human eyes. In this paper, the multitemporal L-band PALSAR and Google Earth images were collected to recognize potential red-bed landslides in Nanjiang County, northeastern edge of the Sichuan Basin, China. Detailed field investigations [22] were performed for the landslide validations and interpretations. This study proves the potential of SAR images in the monitoring of red-bed landslides.

2. Study Area and Data

The study area (Figure 1) is located in the Ta-pa Mountains, northeast of Sichuan province. It belongs to the junction of an arc-shaped tectonic belt and the parallel fold belt in the eastern Sichuan. The red-bed layer mainly consists sand mudstone, which is porous, low-intensity, vulnerable to pressure, and environmental change. The topography is characterized by high mountains and deep ravines, with elevations approximately ranging from several hundred to 2000 meters. Nevertheless, there are also large area gently inclined red beds, on which many farmlands and residences are distributed. The developed river system continuously changes the stability of adjacent slope and the state of groundwater, and under the red beds, the groundwater mainly exists in the form of pore water, which would vary greatly as seasons [11]. This place is controlled by subtropical monsoonal climate, with the annual mean air temperature about 16.2°C and yearly precipitation of 1200 mm. 80% of the rainfall is concentrated in the period from May to October, which is also the high-incidence season for red-bed landslides. More than 1800 landslides were found in the Nanjiang country in 2011, threatening tens of thousands of people's lives and causing huge economic losses.

Twenty-three scenes of L-band ALOS\PALSAR images, for the period from January 2007 to March 2011, were collected from Alaska Satellite Facility for the monitoring of unstable slopes. Radar waves with this long wavelength (about 23.6 cm) can penetrate the vegetation cover, making us acquire the backscattering signal from the ground and coherent interferograms. Table 1 shows the acquisition day of every image in the format of year-month-day. The PALSAR images were in the Stripmap mode (with pixel spacing of about 4.68 m and 3.17 m in range and azimuth directions, respectively), HH polarization, and ascending orbit. The one arc-second (30 m posting) Shuttle Radar Topography Mission (SRTM) digital elevation model (DEM) was downloaded for the topographic phase removal and geocoding. Atmospheric delay products acquiring from GACOS (The Generic Atmospheric Correction Online Service http://www.gacos.net/) were used to remove the atmospheric effect in mountainous regions. Historic google earth images (optical) were used for the underlying graphs of exhibition and recognitions of potential landslides.

Additionally, several high-resolution UAV images and photos were provided as evidences, and detailed field investigations were carried out to integrate the experiment. Common topographic features and deformation characteristics of landslide, such as armchair landform, faulted platform, tension crack, bulging deformation, saber tree, cracking, and deformation of structures, are used to identify and delineate the potential hidden hazard area and qualitatively identify the landslide on the macro level.

3. MTInSAR Methodology

It is difficult to detect enough Permanent Scatterers (PSs) in the vegetation-covered mountains like this study area. Thus, to improve the density of measurable targets, an enhanced SBAS technique was adopted for the potential landslide monitoring [23]. Multilook operation and small-baseline pair method could reduce the effect of decorrelation, and further a phase optimization approach was used to improve the signal-to-noise ratio of interferograms. Considering that moisture would affect the propagation of radar signal and cause disordered fringes on the interferograms especially in mountainous regions, this study used GACOS products to correct the atmospheric delays [24, 25]. Additionally, a biquadratic model was applied to remove the orbital phase errors are common in the L-band InSAR data. The whole processing flowchart can be seen in Figure 2.

First, preprocessing and conventional InSAR were conducted on all SAR acquisitions, mainly for calibration, coregistration, baseline estimation, multilooking, and interferogram generation. The coregistration error is required smaller than 0.2 pixel. Meanwhile, flat earth and topography-related phases were removed through modeling and matching the external SRTM DEM. Second, a crucial process called CAESAR was used for phase optimization to improve the qualities of differential interferograms, and the details can be seen in [26]. The method for identifying homogeneous pixels in adjacent extents is carrying Kolmogorov–Smirnov test on multitemporal magnitude information of each pixel. Optimized phases were estimated to replace their original values in the interferograms. Based on these operations, we got high coherence in the mountainous areas of this study.

Third is the SBAS-related processing. A total of 45 interferometric pairs characterized by small spatial (threshold: 2000 m) and temporal baselines (threshold: 500 days) were generated, followed by computing temporal and spatial coherence of each pixel. Those pixels whose values higher

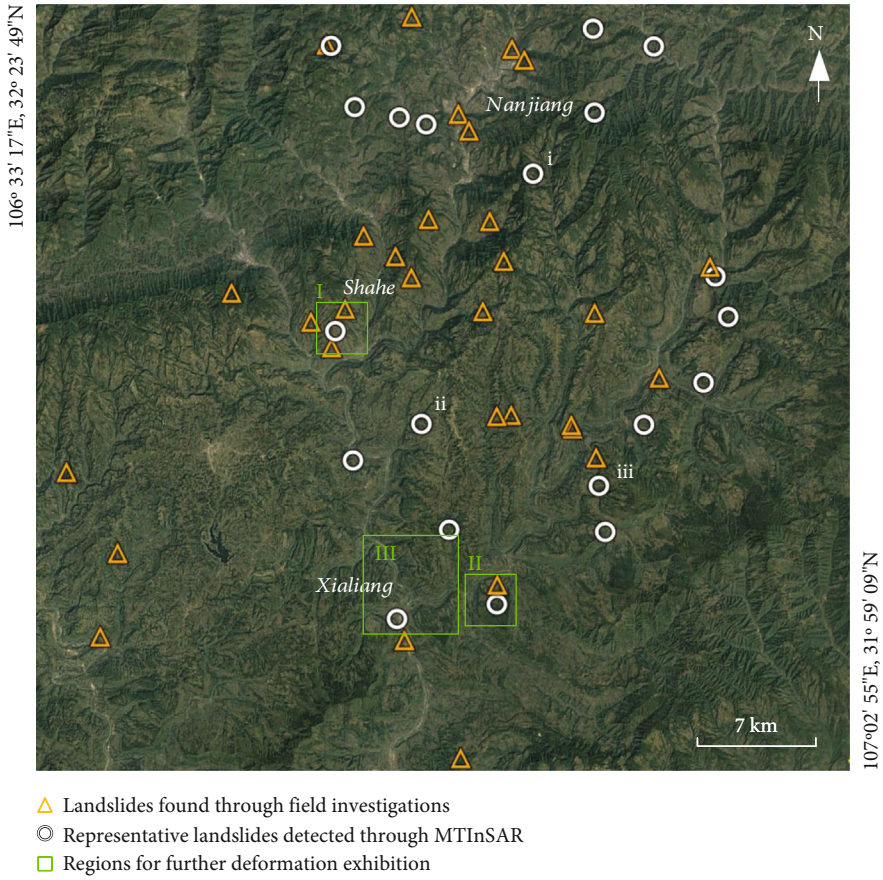

Figure 1: Google Earth image of the study area, on which landslides found through field investigations and MTInSAR were exhibited. Three high-risk regions (from I to III) and small landslide slopes (from i to iii) were indicated to show their deformation results and for further interpretations.

Table 1: Acquisition time of 23 images (format of year-month-day).

2007-01-06	2007-02-21	2007-07-09	2007-08-24	2007-10-09
2007-11-24	2008-01-09	2008-02-24	2008-05-26	2008-11-26
2009-01-11	2009-02-26	2009-07-14	2009-08-29	2009-10-14
2010-01-14	2010-03-01	2010-07-17	2010-09-01	2010-10-17
2011-01-17	2011-03-04			

than 0.5 were selected as measurable candidates, and finally, about 4 million points were kept. A reference point located at flat urban region was chosen. Atmospheric delay effect is serious and common in mountainous regions and would greatly reduce the precision of deformation estimation in a very large scale. Fortunately, GACOS products are capable to provide a good solution which has been proved in previous studies. The data were first applied and downloaded according to the acquisition times and geographic position, resampled to the geometric coordinates of SAR images, and removed from interferograms.

Finally, the minimum cost flow algorithm was adopted for phase unwrapping of differential interferograms. Orbit errors, which are significant in the long-wavelength images, were removed using the methods by Shirzaei and Walter [27]. Through the SVD method, we obtained the deformation rate and residual height of each detected point. Note that iteration strategy should be adopted in the phase unwrapping, various error removal, and parameter estimation till the results remain stable. Then, time series displacements were estimated in the dimension of single-master interferograms. After above, all measurable points were geocoded and imported into the Google Earth images for visualization, with the deformation rate value represented by its color.

Unstable slopes can be found on the MTInSAR-derived deformation map, and then, they were validated and further interpreted through high-resolution optical images and field investigations. Potential red-bed landslides have clear distribution features. Over the Nanjiang County, more than 80% landslides occurred in the (approximately) single–sided or table-shaped mountains, soft and hard interbedded clastic rocks, altitudes between 500 m and 1000 m, gradients from 0 to 20°, and close to the rivers [11]. There are also several landslide identification masks on the optical images. The first is the demarcation line of the vegetation density between landslide bodies and natural surfaces, usually in the shape of irregular circle, and another is the stepped landform especially generated by the old landslide. The ground marks mainly include developed cracks along the gradient,

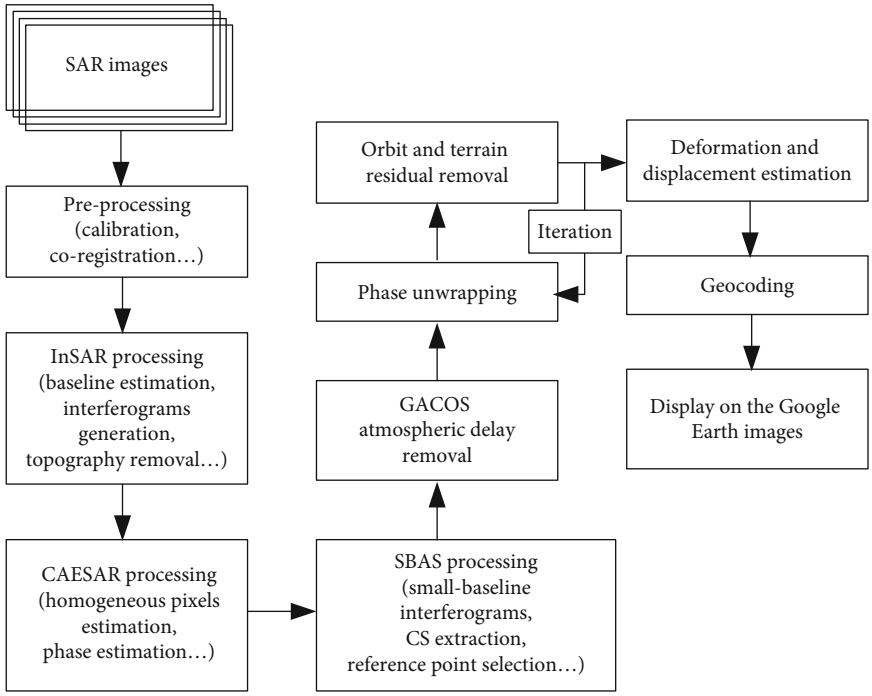

Figure 2: Flowchart of enhanced SBAS technique in this study.

with thickness of the overburden (1 ~ 5 m), better free space conditions (such as scarps and deep gullies), and large-area smooth outcrops [5].

4. Experimental Results and Analysis

According to the MTInSAR-derived results, the majority of the study area was stable except for dozens of slopes which were detected to develop in the Line Of Sight (LOS) direction with a maximum rate of -40 mm/year in the Line Of Sight (LOS) direction. Figure 1 illustrates the representative potential landslide and shows the landslide traces found in field investigations. Their distributions are not strictly identical due to the difference in occurrence time, measure limitations of field investigations (e.g., difficulty to find small displacements and rough terrain to arrive), and InSAR techniques (e.g., few signals in the dense vegetation, layover, and shadow area). Due to the large coverage and huge point numbers, it is difficult to show all point information in one figure and simultaneously preserve interesting details. Thus, for convenience and better visibility, deformation results of several important landslide regions (see Figure 1) rather than the whole study area were exhibited.

4.1. Shahe Landslides. According to the field investigations, Shahe Town is a high-risk place of red-bed landslides. Figure 3 shows one typical case of this town, which is the southern slope of an approximately single-side mountain, moderately cut by rivers at three sides. Based on the terrain features, the range of coverage on the Google Earth images was drawn (see the pinky shadow zone in Figure 3(a), about 4.9 km^2). The slope is relatively gentle with the maximum altitude difference less than 300 m, and a large amount of bench terraces are distributed along the slope. Its upper part is covered by the loose overburden, and the underneath is composed of argillaceous siltstone. On the deformation map (Figure 3(a)), four unstable regions are found, of which the biggest region is located at the left part of the slope. Its approximately triangular shape is consistent well with the tree lines shown in the optical image (see Figure 3(b)). The topography boundary between this triangle region and its surroundings is clear, and thus, it may turn into a single landslide hazard. It should be noted that the construction activity on the top could accelerate the process. Another instability is in the right side of the slope (see Figure 3(c)), just above the downtown area. The historic images show that it was caused by the reclamation at the lower place, and its threat to the residence cannot be ignored either.

4.2. Yaochangping Landslide. Figure 4 shows a slope of Yaochangping on which landslide imprints were discovered in the field investigation. It is fan-shaped, facing south, with the area of about 5 km^2, and altitudes ranging from 400 to 1000 m. On the deformation map, several unstable regions were marked, among which the most serious region is found in the mountain-top covered by natural vegetation. Google Earth images (Figure 4(b)) show that the surface has been cut into pieces by rainfall-induced streams or previous landslides, which result in the strip-shaped distribution of measurable points. Compared with the high-altitude regions, the farmland and buildings are concentrated on the lower and gentler surface. Though most of these regions are relatively stable according to deformation results, several cracks in the farmland, collapsed buildings, and subsiding zones are also found (Figure 4(c)). Especially in September 2011 (almost 6 months after SAR acquisitions), a long-time heavy

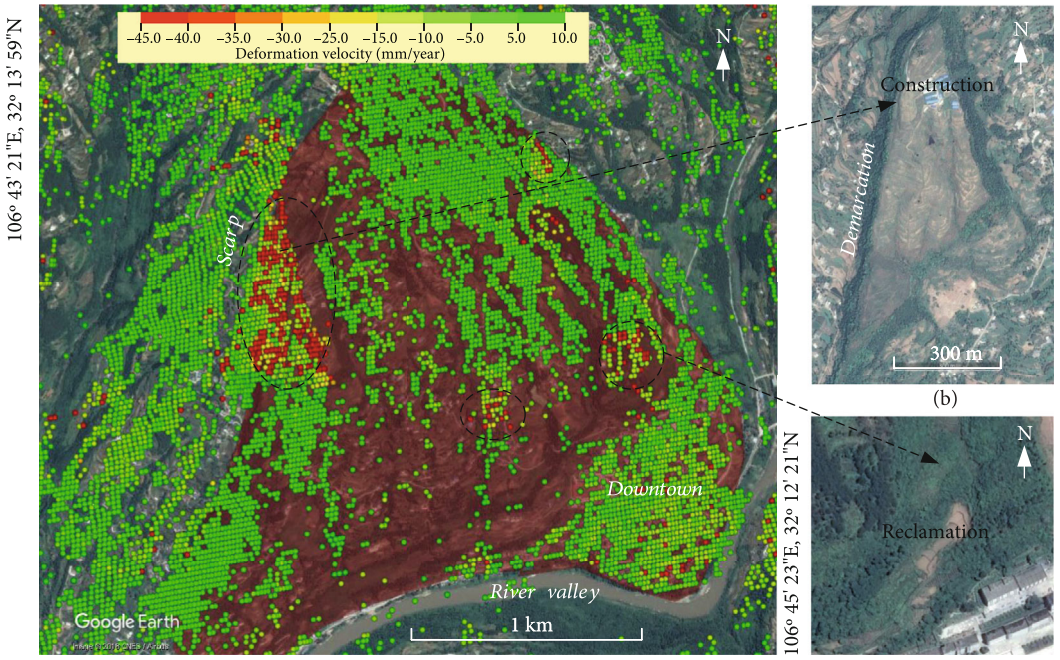

Figure 3: A landslide slope (the pinky shadow zone) in the Shahe Town (region I in Figure 1). (a) The deformation rate map, with four unstable regions indicated by black dotted lines. (b, c) Google Earth images of two unstable places.

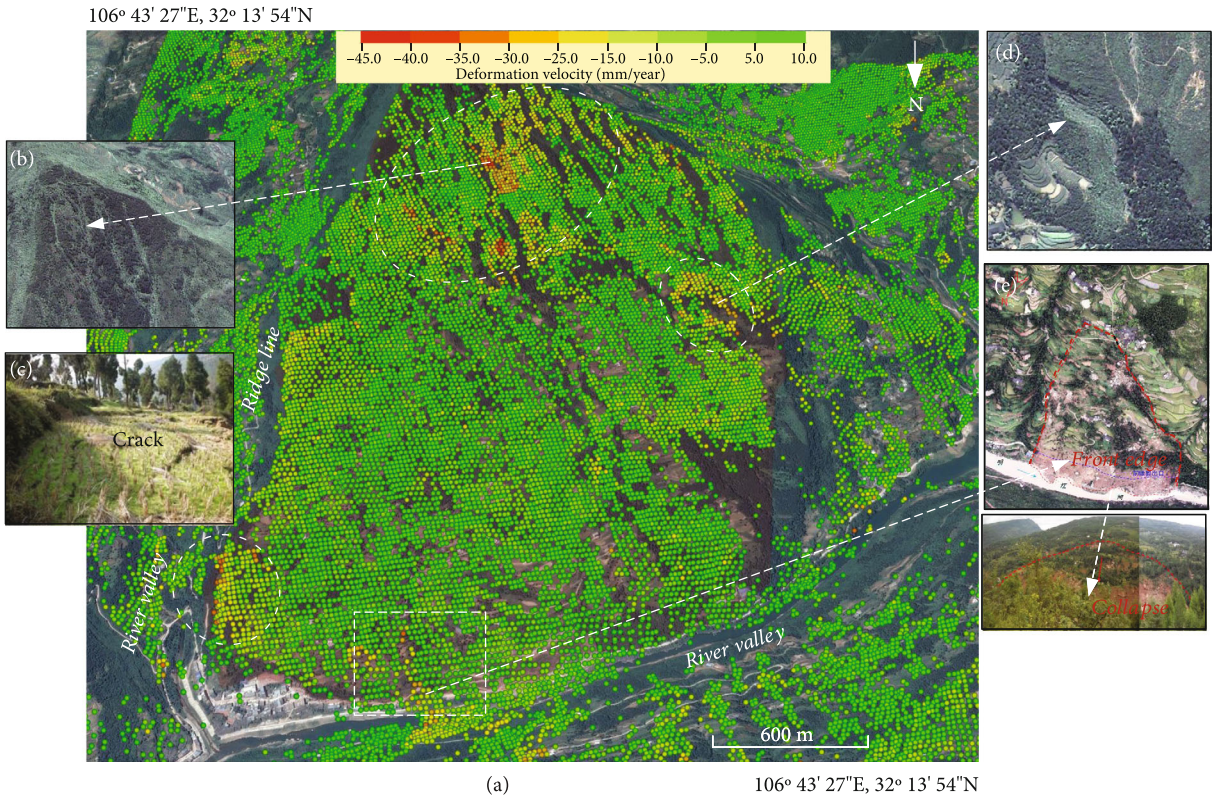

Figure 4: A landslide slope in the Yaochangping (region II in Figure 1). (a) The deformation rate map, with unstable regions indicated by white dotted lines. (b) The Google Earth image (2007.04). (c) A field photo showing cracks. (d) A Google Earth image showing the imprint of an old landslide (2007.04). (e) The UAV image of the landslide (2011.09) with a field collapse photo.

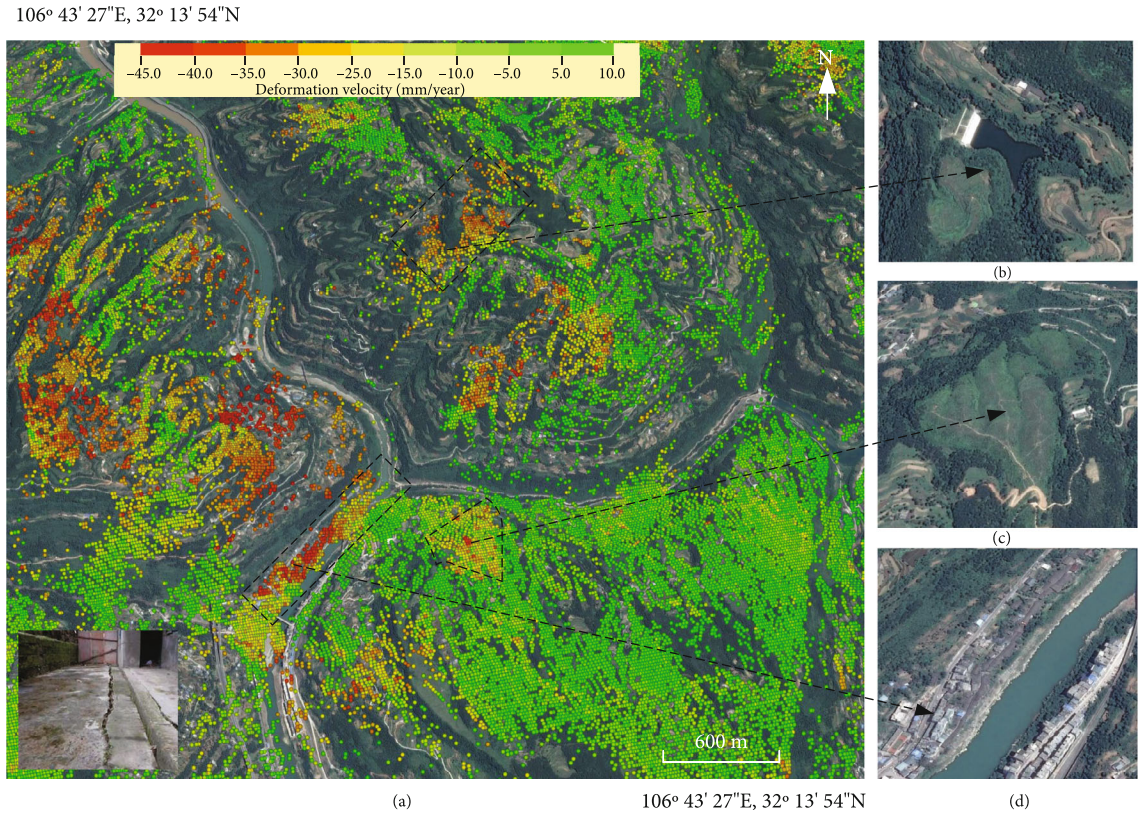

Figure 5: (a) Deformation rate map with a field photo of crack (region III in Figure 1). (b–d) Google Earth images (2013.04).

rainfall caused a fatal large-scale landslide, with the length over 650 m and mean thickness of about 15 m. Figure 4(d) is an old deep landslide with large-volume and length of 150 m, and its edges were detected unstable using InSAR, indicating that the landslide extent was expanding. Figure 4(e) is the UAV image with a field collapse photo. Investigators considered the slope as a giant landslide and outlined it using red lines. We can see that large mass of deposits almost blocked the river, and the foot side of the landslide was still loose.

4.3. Xialiang Landslides. Xialiang Town is located in the south of Nanjiang County, where low mountains, rivers, and red bed landslides are well-developed. Except for a few scarps, most slopes are gentle and beneficial to farming and construction. The strata mainly include the Quaternary Holocene artificial fill, residual soils, landslide accumulation layer, and Jurassic mudstone. The deformation map is shown in Figure 5(a), and it is clearly that the large-area ground here is unstable, especially those high-altitude gentle slopes where human activities are frequent. This phenomenon is validated through field investigation, and we found serious cracks on the ground and walls of a middle school. Its deformation mode belongs to the type of "creep-pull" with tensional cracks in both the front and back edges of the landslide. In the front edge, construction first led to the appearance of free space, and shear cracks developed under the influence of continuing rain and flow of rock water, and then, failure occurred. Subsequently, local slopes slid forward, and cracks formed in the back edge. In Figure 5 (b), a reservoir was constructing and storing up water, and significant changes of land-use reduced the surface capacity to pressure and led to the serious subsiding. Figure 5(c) shows an unstable slope whose geography and vegetation boundaries are obvious. Apart from high-altitude slopes, insecurities were also found on some buildings in the river valley. Figure 5(d) shows a long and narrow residential area built along the river. Serious subsidence can be attributed to the loose soil property and unstable foundations of new-built houses.

4.4. Other Landslides. Through the MTInSAR-derived deformation maps, some high-risk slopes can also be detected which were not found in field investigations and never reported to the government. Figure 6 shows three typical red-bed landslides with their locations indicated in Figure 1 (from i to iii). In Figure 6(a), two discrete slopes are revealed unstable, and Google Earth images show that above them two pieces of bench terraces are developed. Thus, it can be inferred that the farming activities caused the instability. Besides, large unstable regions are detected on the slope of Figure 6(b), where surface water (including reservoir and pools) develops well and cuts the surface into pieces. Many layered arrow-shaped features arrange in several columns on the satellite images. Similarly, the erosion of water would lead to the loose soil property and induce cracks or landslides. Note that the influence of water cycle on landslide has been studied [28]. Most unstable points

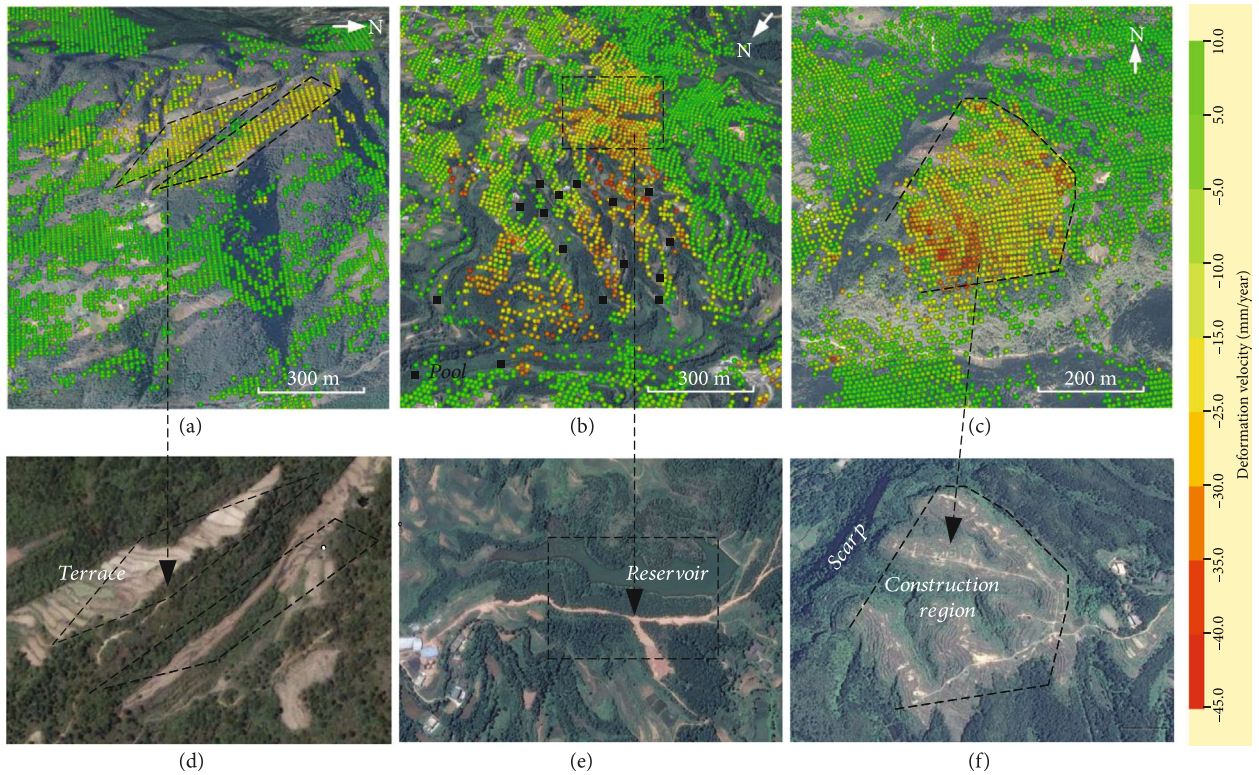

Figure 6: Deformation rate map of other landslides. (a–c) Deformation rate maps of three typical landslide regions (from i to iii in Figure 1). In (b), the locations of pools were marked. (d, e) Google Earth images.

are concentrated near a reservoir (black square in Figure 6 (b)), indicating that the water project is especially dangerous on this kind of slope. In Figure 6(c), there is a whole piece of highland exhibiting unstable indication, which can be attributed to the giant reclaim activities for the crop planting.

5. Discussion

In this study, most MTInSAR-derived red-bed landslides were attributed to human activities, which can be found and verified in the optical images as above examples. However, another consensus is that rainfall should be mainly responsible for the striking landslide disasters and damages, like collapses, rockfalls, and debris flows. This is not contradictory because these emergencies are beyond the reach of MTInSAR techniques, which are good at monitoring the long-term slow-moving landslides. Large-scale sudden movements tend to cause decorrelation and unwrapping errors in the interferograms, making them difficult to measure [29]. That is why MTInSAR results cannot agree well with the government hazard reports. Additionally, geologic tectonics affect the study area little because it is away from the active faults. According to official statistics of Sichuan Earthquake Administration, majority of historic earthquake events in Sichuan occurred in the regions with longitude smaller than 104°E, while the longitudes of the study area are between 106°E and 107°E.

Field investigations are also difficult to entirely prove MTInSAR results, because the former mainly focus on the landform morphology like the sliding traces or cracks and cannot detect the slow movements (perhaps several mm or cm per year). Installing GNSS instrument on slopes to monitor for a long time can verify the MTInSAR results theoretically. However, it is very expensive, localized, and restricted to the errors in position matching with the SAR images. Optical remote sensing images are commonly used to map the previous landslides. In brief, above tools are complementary in monitoring the landslides and jointly contribute to the risk assessment.

6. Conclusion

Red-bed landslides are widely distributed over the Sichuan province, China, and have caused many casualties and economic losses. It is difficult to comprehensively and timely monitor them over the large rugged mountains using traditional field methods. MTInSAR can be used as an effective supplement due to the advantages of large coverage, fast imaging, and low time/financial cost. Through the experiment, we can conclude that the strategy of small baseline in generating interferograms is good for the landslide monitoring; phase optimization could greatly improve the qualities of interferograms in dense vegetation regions; atmospheric delay effects are serious and need to be removed in the mountains. Dozens of potential landslides were recognized, among which some were never found and reported to the government before. Several geological indicators for red-bed landslide occurrences can be concluded as follows:

(1) (Approximately) single–sided or table-shaped mountains

(2) Slope is between 10 and 20 degrees

(3) Effectively exposed and out-dip slope (like the steep ridge in river valley)

(4) Tensional cracks develop on the slope

(5) Gentle soft layers develop on the lower part of slope

This study proves that in red-bed regions MTInSAR has potentials to detect the small displacements caused by human activities, like the construction, reclamation, and irrigation. Optical images and field investigations are mainly used to find large-scale previous events. To predict the rainfall-induced landslides with little warning signs is still a challenging job.

Data Availability

The data used to support the findings of this study are included in the article.

Conflicts of Interest

There is no conflict of interest in this study.

Acknowledgments

This research was financially supported by the Sichuan Science and Technology Project under grant No. 18ZDYF3431, the project of China Geological Survey-Investigation of Urban Geological Disasters in Ta-pa Mountains Area under grant No. DD20160278, and the National Natural Science Foundation of China under Grant No. 41601465.

References

[1] R. Xu and J. Zhou, *Red Bed and Dam (in Chinese)*, China University of Geosciences Press, Wuhan China, 2010.

[2] J. Chen, F. Dai, L. Xu et al., "Properties and microstructure of a natural slip zone in loose deposits of red beds, southwestern China," *Engineering Geology*, vol. 183, pp. 53–64, 2014.

[3] X. M. Fan, Q. Xu, Z. Y. Zhang, S. Dong, and R. Tang, "Study on genetic mechanism of translational landslide," *Chinese Journal of Rock Mechanics and Engineering*, vol. 27, no. 2, pp. 3753–3759, 2008.

[4] J. Chen, X. Li, and Z. Yang, "Baota landslide in the three gorges area and its OSL dating," *Environmental Geology*, vol. 54, no. 2, pp. 417–425, 2008.

[5] J. S. Yi, *Study on Forming Condition and Early Identification of Red Layer Landslide in the East of Sichuan (in Chinese)*, Chengdu University of Technology, Chengdu China, 2015.

[6] X. L. Li, S. J. Chen, Q. M. Zhang, X. Gao, and F. Feng, "Research on theory, simulation and measurement of stress behavior under regenerated roof condition," *Geomechanics and Engineering*, vol. 26, no. 1, pp. 49–61, 2021.

[7] Y. G. Zhang, X. Q. Chen, R. P. Liao et al., "Research on displacement prediction of step-type landslide under the influence of various environmental factors based on intelligent WCA-ELM in the three gorges reservoir area," *Natural Harzard*, vol. 107, no. 2, pp. 1709–1729, 2021.

[8] M. Zhang, Y. Yin, and B. Huang, "Mechanisms of rainfall-induced landslides in gently inclined red beds in the eastern Sichuan Basin, SW China," *Landslides*, vol. 12, no. 5, pp. 973–983, 2015.

[9] Z. M. Hu, *Study on Formation Mechanism of the Slow-Inclination Landslide in Red Stratum Region, Sichuan (in Chinese)*, Chengdu University of Technology, Chengdu China, 2013.

[10] J. M. Kong and Z. S. Chen, "The translational landslide in red stratum located in East Sichuan in July," *Landslide column*, vol. 9, pp. 36–42, 1989.

[11] Y. H. Lu, *Study on Formation Mechanism and Early Identification of Two Free Faces of Red Bed Landslides in Nanjiang (in Chinese)*, Chengdu University of Technology, Chengdu China, 2016.

[12] J. B. Yan, Z. X. Zou, R. Mu et al., "Evaluating the stability of Outang landslide in the three gorges reservoir area considering the mechanical behavior with large deformation of the slip zone," *Natural Hazards*, 2022.

[13] C. Colesanti and J. Wasowski, "Investigating landslides with space-borne synthetic aperture radar (SAR) interferometry," *Engineering Geology*, vol. 88, no. 3-4, pp. 173–199, 2006.

[14] S. Lee, "Application of logistic regression model and its validation for landslide susceptibility mapping using GIS and remote sensing data," *International Journal of Remote Sensing*, vol. 26, no. 7, pp. 1477–1491, 2005.

[15] G. Metternicht, L. Hurni, and R. Gogu, "Remote sensing of landslides: an analysis of the potential contribution to geo-spatial systems for hazard assessment in mountainous environments," *Remote Sensing of Environment*, vol. 98, no. 2-3, pp. 284–303, 2005.

[16] A. Ferretti, C. Prati, and F. L. Rocca, "Permanent scatterers in SAR interferometry," *IEEE Transactions on Geoscience & Remote Sensing*, vol. 39, no. 1, pp. 8–20, 2001.

[17] P. Berardino, G. Fornaro, R. Lanari, and E. Sansosti, "A new algorithm for surface deformation monitoring based on small baseline differential SAR interferograms," *IEEE Transactions on Geoscience & Remote Sensing*, vol. 40, no. 11, pp. 2375–2383, 2002.

[18] A. Ferretti, A. Fumagalli, F. Novali, C. Prati, F. Rocca, and A. Rucci, "A new algorithm for processing interferometric data-stacks: SqueeSAR," *IEEE Transactions on Geoscience & Remote Sensing*, vol. 49, no. 9, pp. 3460–3470, 2011.

[19] X. Shi, L. Zhang, Y. Zhong, L. Zhang, and M. Liao, "Detection and characterization of active slope deformations with Sentinel-1 InSAR analyses in the southwest area of Shanxi, China," *Remote Sensing*, vol. 12, no. 3, p. 392, 2020.

[20] T. Strozzi, P. Farina, A. Corsini et al., "Survey and monitoring of landslide displacements by means of L-band satellite SAR interferometry," *Landslides*, vol. 2, no. 3, pp. 193–201, 2005.

[21] J. Wasowski and F. Bovenga, "Investigating landslides and unstable slopes with satellite multi temporal interferometry: current issues and future perspectives," *Engineering Geology*, vol. 174, pp. 103–138, 2014.

[22] X. Wang, Y. Xiao, W. Shi et al., "Forensic analysis and numerical simulation of a catastrophic landslide of dissolved and fractured rock slope subject to underground mining," *Landslides*, pp. 1–23, 2022.

[23] P. Tang, F. Chen, H. Guo, B. Tian, X. Wang, and N. Ishwaran, "Large-area landslides monitoring using advanced multi-

temporal InSAR technique over the giant panda habitat, Sichuan, China," *Remote Sensing*, vol. 7, no. 7, pp. 8925–8949, 2015.

[24] Q. Wang, W. Yu, B. Xu, and G. Wei, "Assessing the use of GACOS products for SBAS-INSAR deformation monitoring: a case in Southern California," *Sensors*, vol. 19, no. 18, p. 3894, 2019.

[25] C. Yu, Z. Li, N. T. Penna, and P. Crippa, "Generic atmospheric correction model for interferometric synthetic aperture radar observations," *Journal of Geophysical Research: Solid Earth*, vol. 123, no. 10, pp. 9202–9222, 2018.

[26] G. Fornaro, S. Verde, D. Reale, and A. Pauciullo, "Caesar: an approach based on covariance matrix decomposition to improve multibaseline–multitemporal interferometric SAR processing," *IEEE Transactions on Geoscience & Remote Sensing*, vol. 53, no. 4, pp. 2050–2065, 2015.

[27] M. Shirzaei and T. R. Walter, "Estimating the effect of satellite orbital error using wavelet-based robust regression applied to InSAR deformation data," *IEEE Transactions on Geoscience and Remote Sensing*, vol. 49, no. 11, pp. 4600–4605, 2011.

[28] Y. G. Zhang, J. Tang, R. P. Liao et al., "Application of an enhanced BP neural network model with water cycle algorithm on landslide prediction," *Stochastic Environmental Research and Risk Assessment*, vol. 35, no. 6, pp. 1273–1291, 2021.

[29] S. Moretto, F. Bozzano, and P. Mazzanti, "The role of satellite InSAR for landslide forecasting: limitations and openings," *Remote sensing*, vol. 13, no. 18, p. 3735, 2021.